Article

Not peer-reviewed version

Identification of Electrostatic Hotspots at the Binding Interface of Amylin and Insulin-Degrading Enzyme: A Structural and Biophysical Investigation

Wei Li *

Posted Date: 1 February 2024

doi: 10.20944/preprints202402.0063.v1

Keywords: Amylin; Insulin-degrading enzyme; Electrostatic hotspots; Salt bridge; Hydrogen bond

 doi:10.20944/preprints202402.0063.v1

Article

Identification of Electrostatic Hotspots at the Binding Interface of Amylin and Insulin-Degrading Enzyme: A Structural and Biophysical Investigation

Wei Li

Contrebola Institute of Computational Interstructural Biophysics, No. 88, Fuxing East Road, Nantong City 226000, Jiangsu Province, People's Republic of China; wli148@aucklanduni.ac.nz

Abstract: Amylin, also known as islet amyloid polypeptide (IAPP), is a metabolic homeostasis-related hormone that is produced and released by the β cells of the pancreas, the same cells that produce insulin. Insulin-degrading enzyme (IDE) is a protease enzyme that plays an essential role in the breakdown and degradation of various peptides, including insulin and amylin. Direct binding & interaction between amylin and IDE is inextricably linked to the degradation of amylin, and research and development effort in this area is crucial to understand the potential therapeutic implications of disrupting the IDE-amylin interaction in the context of conditions where metabolic homeostasis needs to be regulated, such as diabetes and obesity. Here, this article incorporates currently available experimental complex structure of amylin and IDE, and delves deep into the interstructural biophysics underlying the binding interface of the two interacting partners. With a set of comprehensive structural biophysical analysis, this article identified an intriguing region of high electrostatic potential indicative of strong binding sites between the first N-terminal lysine (Lys1, K1) residue of amylin and Glu341 (E341) of IDE. This unique electrostatic hotspot presented herein paves the way for the rational design of drug-like small molecules that can selectively disrupt this interaction, offering a targeted therapeutic strategy for improved metabolic homeostasis, particularly for patients with diabetes and obesity.

Keywords: amylin; insulin-degrading enzyme; electrostatic hotspots; salt bridge; hydrogen bond

1. Introduction

Amylin is a 37-amino-acid pancreatic hormone acting to control energy homeostasis and body weight [1–4]. Physiologically, amylin regulates glucose homeostasis by inhibiting insulin and glucagon secretion [5–7]. Furthermore, amylin modulates satiety and inhibits gastric emptying via the central nervous system [8–11]. Produced and released by pancreatic β cells, amylin shares a common secretion pathway with insulin, collectively orchestrating the postprandial control of glucose homeostasis [12–15]. The intricate regulatory network governing blood sugar levels involves a delicate interplay between hormones and enzymes, among which amylin (islet amyloid polypeptide, IAPP) and insulin-degrading enzyme (IDE) stand as key players [12,16–21], where IDE plays a crucial role in the degradation and clearance of amylin from the bloodstream [22–24]. The cooperation between amylin and IDE, therefore, is pivotal in maintaining the delicate balance of glucose homeostasis and averting the detrimental consequences of amyloid deposition [25–29]. For instance, IDE defects are linked to the development of type 2 diabetes mellitus (T2DM) and Alzheimer's disease (AD) [13,18,30].

2. Motivation

Thanks to the continued development of experimental structural biology and the half-a-century old Protein Data Bank (PDB) [31,32], a comprehensive structural biophysical (CSB) analysis becomes possible [33–35] for specific ligand-receptor [36–38], antigen-antibody [39] or enzyme-substrate [40–42] complex structures deposited in PDB, expanding our understanding of the structural and biophysical

 doi:10.20944/preprints202402.0063.v1

basis of their interfacial structural stability, and facilitating the design of drug analogues with improved affinity to their interacting partners [43,44].

As a matter of fact, structural and biochemical analyses [45–48] have already revealed the binding mode and pattern for the formation of the IDE-amylin complex structure, and this experimental information is useful but insufficient for the development of promising inhibitors (e.g., small molecules) of IDE-amylin interaction to improve glucose homeostasis. This manuscript, therefore, seeks to delve into the structural and biophysical aspects of the interaction between amylin and IDE, with a specific focus on identifying electrostatic hotspots at their binding interface. In case these hotspots are able to act as potential binding sites for drug-like small molecules, the aim of this article is to provide a precise and targeted approach for the development of small molecules to disrupt the amylin-IDE interaction.

3. Materials and Methods

As of February 1, 2024, a total of 101 experimental structures have been deposited in Protein Data Bank (PDB) [31] as listed in Table 1, according to a text query: QUERY: Full Text = "amylin" of the Protein Data Bank (PDB) [31]. Among them, only two experimental structures represent the amylin-IDE complex, with PDB IDs: 2G48 [45,46] and 3HGZ [47,48], respectively, providing an accurate structural basis of the IDE-amylin interaction specificity for subsequent comprehensive structural biophysical (CSB) analysis of the two structural models (two yellow rows in Table 1).

First, after the atomic coordinates file for PDB IDs: 2G48 [45,46] and 3HGZ [47,48] were downloaded from the PDB [31] website, Chimera [49] was employed to manually add hydrogen atoms to the structural model of the two structural models representing IDE-amylin complex. Afterwards, the two hydrogen-added structural models were subject to a set of comprehensive structural biophysical (CSB) analysis as described in [33] to identify key residue-specific interactions at the amylin-IDE binding interface and uncover the interstructural biophysics underlying the IDE-amylin complex structure.

Specifically, the CSB analysis here [33] consists of the structural identification of salt bridges and side chain hydrogen bonds at the binding interface of amylin and IDE. Given the fact that native proteins are in dynamic equilibrium with their less-structured, partially folded and/or unfolded states [50], and that, according to an NMR structure of human amylin bound to model membranes, the α helix structure of amylin itself is also dynamic, this article uses two sets of screening criteria for the structural identification of potential hotspots at the IDE-amylin binding interface in the two structural models i.e., PDB IDs: 2G48 [45,46] and 3HGZ [47,48].

First, the same set of criteria as in [33] was used, i.e., the interfacial salt bridge analysis was conducted with an in-house python script only for titrateable residues (Asp, Glu, Lys, Arg and His), 4.0 Å was used as the cutoff distance for the two oppositely charged groups [33,51]. The hydrogen bond analysis was also conducted for only side chain nuclei with an in-house python script, and employed two geometric criteria: (a) a cutoff value of the angle formed by acceptor (A), donor (D) and hydrogen (H) ($\angle ADH$) of 30°; (b) a cutoff value of donor-acceptor distance at 3.0 Å. That is, a hydrogen bond is only considered to be formed if $\angle ADH$ is not larger than 30° and the donor-acceptor distance is not larger than 3.0 Å [33,51].

Afterwards, a new set of criteria was used to account for the dynamic α-helix structure of amylin itself, i.e., the interfacial salt bridge analysis was conducted with an in-house python script only for titrateable residues (Asp, Glu, Lys, Arg and His), 6.0 Å was used as the cutoff distance for the two oppositely charged groups [33,51]. The hydrogen bond analysis was also conducted for only side chain nuclei with an in-house python script, and employed two geometric criteria: (a) a cutoff value of the angle formed by acceptor (A), donor (D) and hydrogen (H) ($\angle ADH$) of 50°; (b) a cutoff value of donor-acceptor distance at 5.0 Å. That is, a hydrogen bond is only considered to be formed if $\angle ADH$ is not larger than 30° and the donor-acceptor distance is not larger than 5.0 Å [33,51].

 doi:10.20944/preprints202402.0063.v1

Table 1. Experimentally determined amylin-related structures in the Protein Data Bank (PDB [31]) as of February 1, 2024. **QUERY: Full Text = "amylin"**. In this table, the two structural models representing IDE-amylin complex are highlighted in two yellow rows, i.e., PDB IDs: 2G48 [45,46] and 3HGZ [47,48].

PDB ID	Structure Title
8AZ7	IAPP S20G plateau-phase fibril polymorph 4PF-LJ
8AZ6	IAPP S20G plateau-phase fibril polymorph 4PF-LU
8AZ5	IAPP S20G plateau-phase fibril polymorph 4PF-CU
8AZ4	IAPP S20G plateau-phase fibril polymorph 2PF-L
8AZ3	IAPP S20G growth-phase fibril polymorph 4PF-CU
8AZ2	IAPP S20G growth-phase fibril polymorph 3PF-CU
8AZ1	IAPP S20G growth-phase fibril polymorph 2PF-C
8AZ0	IAPP S20G growth-phase fibril polymorph 2PF-L
8AWT	IAPP S20G lag-phase fibril polymorph 2PF-P
8T89	Racemic mixture of amyloid beta segment 16-KLVFFA-21 forms heterochiral rippled beta-sheet
8T86	Racemic mixture of amylin segment 25-AILSS-29 forms heterochiral rippled beta-sheet
8T84	Racemic mixture of amyloid beta segment 35-MVGGVV-40 forms heterochiral rippled beta-sheet, includes hexafluoroisopropanol
8T82	Racemic mixture of amyloid beta segment 35-MVGGVV-40 forms heterochiral rippled beta-sheet, includes pentafluoropropionic acid
8F2B	Amylin 3 Receptor in complex with Gs and Pramlintide analogue peptide San45
8F2A	Human Amylin3 Receptor in complex with Gs and Pramlintide analogue peptide San385 (Cluster 5 conformation)
8F0K	Human Amylin3 Receptor in complex with Gs and Pramlintide analogue peptide San385
8F0J	Calcitonin Receptor in complex with Gs and Pramlintide analogue peptide San45
7YKW	Structure of hIAPP fibril at 3.6 Angstroms resolution
7YL7	Structure of hIAPP-TF-type3
7YL3	Structure of hIAPP-TF-type1
7YL0	Structure of hIAPP-TF-type2
8AX7	Crystal structure of a CGRP receptor ectodomain heterodimer bound to macrocyclic inhibitor HTL0031448
8AX6	Crystal structure of a CGRP receptor ectodomain heterodimer bound to macrocyclic inhibitor HTL0029882
8AX5	Crystal structure of a CGRP receptor ectodomain heterodimer bound to macrocyclic inhibitor HTL0029881
7P0I	Crystal structure of a CGRP receptor ectodomain heterodimer bound to macrocyclic inhibitor Compound 13
7P0F	Crystal structure of a CGRP receptor ectodomain heterodimer bound to macrocyclic inhibitor HTL0028125
7TYX	Human Amylin2 Receptor in complex with Gs and rat amylin peptide
7TYN	Calcitonin Receptor in complex with Gs and salmon calcitonin peptide
7TYI	Calcitonin Receptor in complex with Gs and rat amylin peptide, CT-like state
7TZF	Human Amylin3 Receptor in complex with Gs and rat amylin peptide
7TYY	Human Amylin2 Receptor in complex with Gs and salmon calcitonin peptide
7TYW	Human Amylin1 Receptor in complex with Gs and salmon calcitonin peptide
7TYO	Calcitonin receptor in complex with Gs and human calcitonin peptide
7TYL	Calcitonin Receptor in complex with Gs and rat amylin peptide, bypass motif
7TYH	Human Amylin2 Receptor in complex with Gs and human calcitonin peptide
7TYF	Human Amylin1 Receptor in complex with Gs and rat amylin peptide
7VV0	Cryo-EM structure of pseudoallergen receptor MRGPRX2 complex with PAMP-12, local
7M65	Cryo-EM structure of human islet amyloid polypeptide (hIAPP, or amylin) fibrils seeded by patient extracted fibrils, polymorph 4
7M64	Cryo-EM structure of human islet amyloid polypeptide (hIAPP, or amylin) fibrils seeded by patient extracted fibrils, polymorph 3
7M62	Cryo-EM structure of human islet amyloid polypeptide (hIAPP, or amylin) fibrils seeded by patient extracted fibrils, polymorph 2
7M61	Cryo-EM structure of human islet amyloid polypeptide (hIAPP, or amylin) fibrils seeded by patient extracted fibrils, polymorph 1
7BG0	Fusion of MBP and the backbone of the long-acting amylin analog AM833.
7KNU	CryoEM structure of the CGRP receptor with bound CGRP peptide in a detergent micelle
7KNT	CryoEM structure of the apo-CGRP receptor in a detergent micelle
6ZRR	three-protofilament amyloid structure of S20G variant of human amylin (IAPP - Islet Amyloid Polypeptide)
6ZRQ	two-protofilament amyloid structure of S20G variant of human amylin (IAPP - islet amyloid polypeptide)
6ZRF	amyloid structure of amylin (IAPP - islet amyloid polypeptide)
6V2E	Crystal structure of the human CLR:RAMP2 extracellular domain heterodimer with bound high-affinity adrenomedullin S45R/K46L/S48G/Q50W variant
6ZIS	Crystal structure of a CGRP receptor ectodomain heterodimer with bound high affinity inhibitor
6ZHO	Crystal structure of a CGRP receptor ectodomain heterodimer with bound high affinity inhibitor
6VW2	Cryo-EM structure of human islet amyloid polypeptide (hIAPP, or amylin) fibrils
6UVA	CryoEM Structure of the active Adrenomedullin 2 receptor G protein complex with adrenomedullin 2 peptide
6UUS	CryoEM Structure of the active Adrenomedullin 2 receptor G protein complex with adrenomedullin peptide
6UUN	CryoEM Structure of the active Adrenomedullin 1 receptor G protein complex with adrenomedullin peptide
6Y1A	Amyloid fibril structure of islet amyloid polypeptide
6UCK	proIAPP in DPC Micelles - Two-Conformer Ensemble Refinement, Bent Conformer
6UCJ	proIAPP in DPC Micelles - Two-Conformer Ensemble Refinement, Open Conformer
6UMG	Crystal structure of erenumab Fab bound to the extracellular domain of CGRP receptor
6PGQ	Crystal structure of N-glycosylated human calcitonin receptor extracellular domain in complex with salmon calcitonin (22-32)
6PFO	Crystal structure of N-glycosylated human calcitonin receptor extracellular domain in complex with salmon calcitonin (16-32)
6NIY	A high-resolution cryo-electron microscopy structure of a calcitonin receptor-heterotrimeric Gs protein complex
6E3Y	Cryo-EM structure of the active, Gs-protein complexed, human CGRP receptor
6D1U	Crystal structure of the human CLR:RAMP1 extracellular domain heterodimer in complex with adrenomedullin 2/intermedin
5V6Y	Crystal structure of the human CLR:RAMP1 extracellular domain heterodimer with bound high-affinity and altered selectivity adrenomedullin variant
5UZ7	Volta phase plate cryo-electron microscopy structure of a calcitonin receptor-heterotrimeric Gs protein complex
5MGQ	Solution structure of oxidized and amidated human IAPP (1-37), the diabetes II peptide.
5KO0	Human Islet Amyloid Polypeptide Segment 15-FLVHSSNNFGA-25 Determined by MicroED
5KNZ	Human Islet Amyloid Polypeptide Segment 19-SGNNFGAILSS-29 with Early Onset S20G Mutation Determined by MicroED
5K5G	Structure of human islet amyloid polypeptide in complex with an engineered binding protein
5II0	Crystal structure of the human calcitonin receptor ectodomain in complex with a truncated salmon calcitonin analogue
4RWG	Crystal structure of the CLR:RAMP1 extracellular domain heterodimer with bound high affinity CGRP analog
4RWF	Crystal structure of the CLR:RAMP2 extracellular domain heterodimer with bound adrenomedullin
3AQE	Crystal structure of the extracellular domain of human RAMP2
3AQF	Crystal structure of the human CRLR/RAMP2 extracellular complex
2L7S	Determination of the three-dimensional structure of adrenomedullin, a first step towards the analysis of its interactions with receptors and small molecules
2L86	Solution NMR structure of human amylin in SDS micelles at pH 7.3
2XVT	Structure of the extracellular domain of human RAMP2
3N7S	Crystal structure of the ectodomain complex of the CGRP receptor, a Class-B GPCR, reveals the site of drug antagonism
3N7R	Crystal structure of the ectodomain complex of the CGRP receptor, a Class-B GPCR, reveals the site of drug antagonism
3N7P	Crystal structure of the ectodomain complex of the CGRP receptor, a Class-B GPCR, reveals the site of drug antagonism
3HGZ	Crystal structure of human insulin-degrading enzyme in complex with amylin
2WK3	Crystal structure of human insulin-degrading enzyme in complex with amyloid-beta (1-42)
2KIB	Protein Fibril
3E50	Crystal structure of human insulin degrading enzyme in complex with transforming growth factor-alpha
3E4Z	Crystal structure of human insulin degrading enzyme in complex with insulin-like growth factor II
3FTR	Structure of an amyloid forming peptide SSTNVG from IAPP (alternate polymorph)
3FTL	NVGSNTY segment from Islet Amyloid Polypeptide (IAPP or Amylin), dehydrated crystal form
3FTK	NVGSNTY segment from Islet Amyloid Polypeptide (IAPP or Amylin), hydrated crystal form
3FTH	NFLVHSS segment from Islet Amyloid Polypeptide (IAPP or Amylin)
3FR1	NFLVHS segment from Islet Amyloid Polypeptide (IAPP or Amylin)
3FPO	HSSNNF segment from Islet Amyloid Polypeptide (IAPP or Amylin)
3G7W	Islet Amyloid Polypeptide (IAPP or Amylin) Residues 1 to 22 fused to Maltose Binding Protein
3G7V	Islet Amyloid Polypeptide (IAPP or Amylin) fused to Maltose Binding Protein
2KJ7	Three-Dimensional NMR Structure of Rat Islet Amyloid Polypeptide in DPC micelles
2KB8	The dynamic alpha-helix structure of micelle-bound human amylin.
3DGJ	NNFGAIL segment from Islet Amyloid Polypeptide (IAPP or amylin)
3DG1	Segment SSTNVG derived from IAPP
2YX8	Crystal structure of the extracellular domain of human RAMP1
2G48	crystal structure of human insulin-degrading enzyme in complex with amylin
2FLY	Proadrenomedullin N-Terminal 20 Peptide
1KUW	High-Resolution Structure and Localization of Amylin Nucleation Site in Detergent Micelle

 doi:10.20944/preprints202402.0063.v1

Here, the in-house python scripts essentially are the same as those used in [52], except for the differences in three key parameters related to the screening criteria, i.e., the salt bridge distance cutoff in Å, cutoff angle $\angle ADH$ in ° for hydrogen bonding, and the cutoff distance (in Å) of donor-acceptor for hydrogen bonding.

4. Results

4.1. Characterization of residue-specific electrostatic interactions at the amylin-IDE binding interface

As of February 1, 2024, there are only two experimental structures representing the amylin-IDE complex, with PDB IDs: 2G48 [45,46] and 3HGZ [47,48], respectively (Table 1). As defined in the PDB format content of PDB IDs: 2G48 [45,46] and 3HGZ [47,48], chains A and B represent IDE in 3HGZ, chains D and E represent amylin in 3HGZ, while chains A and B represent IDE in 2G48, and chains C and D represent amylin in 2G48, respectively. For the two structural models (2G48 [45,46] and 3HGZ [47,48]), this article reports a set of comprehensive structural biophysical (CSB) analysis as described in [33], which lead to a set of residue-specific electrostatic interactions at the binding interface of amylin-IDE, as listed in Tables 2–7. Specifically,

1. 10 interfacial salt bridges (Table 2) were structurally identified for the amylin-IDE complex structure PDB ID 2G48 [45,46], according to the old set of criteria as in [33].
2. of the 10, only 1 interfacial salt bridge (Table 2) was structurally identified at the amylin-IDE binding interface for the amylin-IDE complex structure PDB ID 2G48 [45,46], according to the old set of criteria as in [33].
3. 6 interfacial salt bridges (Table 2) were structurally identified for the amylin-IDE complex structure PDB ID 3HGZ [47,48], according to the old set of criteria as in [33].
4. of the 6, 2 interfacial salt bridges (Table 2) were structurally identified at the amylin-IDE binding interface for the amylin-IDE complex structure PDB ID 3HGZ [47,48], according to the old set of criteria as in [33].
5. 14 interfacial side chain and main chain hydrogen bonds (Table 3) were structurally identified for the amylin-IDE complex structure PDB ID 2G48 [45,46], according to the old set of criteria as in [33].
6. no interfacial side chain or main chain hydrogen bond was structurally identified for the amylin-IDE complex structure PDB ID 3HGZ [47,48], according to the old set of criteria as in [33].
7. 4 interfacial side chain hydrogen bonds (Table 4) were structurally identified for the amylin-IDE complex structure PDB ID 2G48 [45,46], according to the old set of criteria as in [33].
8. no interfacial side chain was structurally identified for the amylin-IDE complex structure PDB ID 3HGZ [47,48], according to the old set of criteria as in [33].

 doi:10.20944/preprints202402.0063.v1

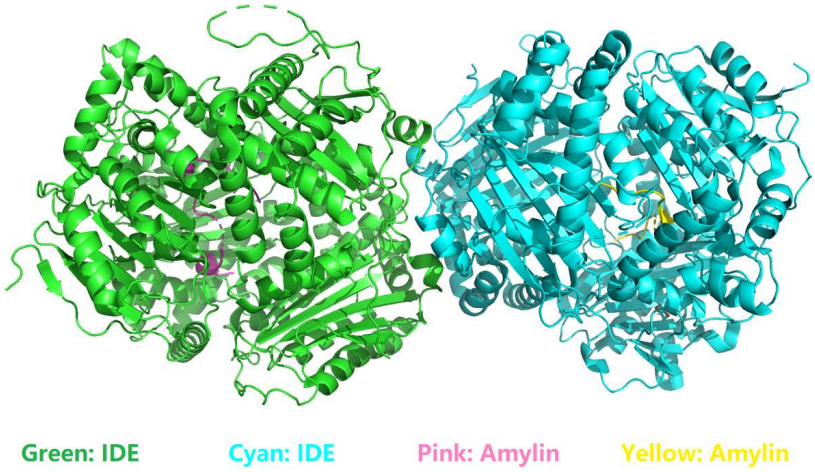

Figure 1. The overall structure of human insulin-degrading enzyme in complex with amylin. This figure is prepared by PyMol [53] with PDB ID 2G48 [45,46]. In this figure, IDE as an amylin-degrading enzyme is like a cage for amylin as its substrate, making it a preferable choice for the potential development of small molecule inhibitor(s) to reach inside IDE (the cage) and disrupt the amylin-IDE interaction for improved metabolic homeostasis.

Table 2. Interfacial salt bridging network analysis of the two structural models of IDE-amylin complex (Table 1), i.e., PDB IDs 2G48 [45,46] and 3HGZ [47,48] according to the old set of criteria as in [33]. In this table, the residue naming scheme is **Chain ID_residue name_residue number**. As defined in the PDB format content of PDB IDs: 2G48 [45,46] and 3HGZ [47,48], chains A and B represent IDE in 3HGZ, chains D and E represent amylin in 3HGZ, while chains A and B represent IDE in 2G48, and chains C and D represent amylin in 2G48, respectively.

PDB ID	Residue A	Atom A	Residue B	Atom B	Distance (Å)
2G48	A_ARG_722	NH1	B_ASP_706	OD1	2.987
2G48	A_ARG_722	NH1	B_ASP_706	OD2	2.560
2G48	A_ARG_722	NH2	B_GLU_702	OE2	3.255
2G48	A_LYS_756	NZ	B_ASP_706	OD1	3.852
2G48	B_ARG_722	NH1	A_ASP_706	OD1	2.728
2G48	B_ARG_722	NH1	A_ASP_706	OD2	3.524
2G48	B_ARG_722	NH2	A_ASP_706	OD1	3.653
2G48	B_LYS_756	NZ	A_ASP_706	OD1	3.253
2G48	B_LYS_756	NZ	A_ASP_706	OD2	2.575
2G48	C_LYS_1	NZ	A_GLU_341	OE1	3.514
3HGZ	A_ARG_164	NH1	B_GLU_408	OE1	3.083
3HGZ	A_ARG_164	NH1	B_GLU_408	OE2	3.662
3HGZ	A_ARG_164	NH2	B_GLU_408	OE1	3.032
3HGZ	B_LYS_327	NZ	A_GLU_880	OE1	3.476
3HGZ	D_LYS_1	NZ	A_GLU_341	OE1	2.441
3HGZ	E_LYS_1	NZ	B_GLU_341	OE1	3.179

 doi:10.20944/preprints202402.0063.v1

Table 3. 2G48-specific interfacial side chain and main chain hydrogen bonding analysis according to the old set of criteria as in [33]. In this table, the residue naming scheme is **Chain ID_residue name_residue number**, $\angle ADH$ represents the angle formed by acceptor (A), donor (D) and hydrogen (H) ($\angle ADH$). As defined in the PDB format content of PDB IDs: 2G48 [45,46] and 3HGZ [47,48], chains A and B represent IDE in 3HGZ, chains D and E represent amylin in 3HGZ, while chains A and B represent IDE in 2G48, and chains C and D represent amylin in 2G48, respectively.

PDB ID	Acceptor (A)	Donor (D)	Hydrogen (H)	D-A (Å)	H-A (Å)	∠ADH(°)
2G48	O, C_LYS_1	N, A_GLY_361	H, A_GLY_361	2.72	1.72	5.66
2G48	OE2, B_GLU_699	OG, A_SER_761	HG, A_SER_761	2.52	1.67	22.41
2G48	O, C_LEU_16	NH2, A_ARG_824	HH21, A_ARG_824	2.98	2.09	22.98
2G48	O, D_ASN_14	N, B_THR_142	H, B_THR_142	2.89	1.99	21.69
2G48	O, D_LYS_1	N, B_GLY_361	H, B_GLY_361	2.89	1.89	5.77
2G48	OD1, A_ASP_706	NH1, B_ARG_722	HH12, B_ARG_722	2.73	1.91	29.32
2G48	OD2, A_ASP_706	NZ, B_LYS_756	HZ1, B_LYS_756	2.57	1.59	10.38
2G48	OE2, A_GLU_699	OG, B_SER_761	HG, B_SER_761	2.51	1.64	19.94
2G48	O, A_GLY_361	N, C_ASN_3	H, C_ASN_3	2.65	1.76	22.83
2G48	O, A_ALA_140	N, C_LEU_16	H, C_LEU_16	2.97	2.01	15.18
2G48	OE1, B_GLU_341	N, D_LYS_1	H2, D_LYS_1	2.85	1.85	6.72
2G48	O, B_GLY_361	N, D_ASN_3	H, D_ASN_3	2.67	1.76	20.40
2G48	O, B_GLN_363	ND2, D_ASN_3	HD22, D_ASN_3	2.73	1.89	26.92
2G48	O, B_ALA_140	N, D_LEU_16	H, D_LEU_16	2.83	1.95	23.79

Table 4. 2G48-specific interfacial side chain hydrogen bonding analysis according to the old set of criteria as in [33]. In this table, the residue naming scheme is **Chain ID_residue name_residue number**, $\angle ADH$ represents the angle formed by acceptor (A), donor (D) and hydrogen (H) ($\angle ADH$). As defined in the PDB format content of PDB IDs: 2G48 [45,46] and 3HGZ [47,48], chains A and B represent IDE in 3HGZ, chains D and E represent amylin in 3HGZ, while chains A and B represent IDE in 2G48, and chains C and D represent amylin in 2G48, respectively.

PDB ID	Acceptor (A)	Donor (D)	Hydrogen (H)	D-A (Å)	H-A (Å)	∠ADH(°)
2G48	OE2, B_GLU_699	OG, A_SER_761	HG, A_SER_761	2.52	1.67	22.41
2G48	OD1, A_ASP_706	NH1, B_ARG_722	HH12, B_ARG_722	2.73	1.91	29.32
2G48	OD2, A_ASP_706	NZ, B_LYS_756	HZ1, B_LYS_756	2.57	1.59	10.38
2G48	OE2, A_GLU_699	OG, B_SER_761	HG, B_SER_761	2.51	1.64	19.94

As discussed above, to account for the dynamic α helix structure and less-structured or random coil region of amylin, this article uses two sets of screening criteria for structural identification of potential electrostatic hotspots at the IDE-amylin binding interface in the two structural models i.e., PDB IDs: 2G48 [45,46] and 3HGZ [47,48]. Specifically,

1. a total of 22 interfacial salt bridges (Table 5) were structurally identified for the amylin-IDE complex structure PDB ID 2G48 [45,46], according to a new set of criteria [33] as defined in the section of Materials and Methods.
2. among the 22, only 3 interfacial salt bridges (Table 5) were structurally identified between Lys1 and Glu341 (Figures 2 and 3) at the binding interface of IDE and amylin for the amylin-IDE complex structure PDB ID 2G48 [45,46], according to a new set of criteria [33] as defined in the section of Materials and Methods.
3. a total of 16 interfacial salt bridges (Table 5) were structurally identified for the amylin-IDE complex structure PDB ID 3HGZ [47,48], according to a new set of criteria [33] as defined in the section of Materials and Methods.
4. among the 16, only 4 interfacial salt bridges (Table 5) were structurally identified between Lys1 and Glu341 (Figures 2 and 3) at the binding interface of IDE and amylin for the amylin-IDE complex structure PDB ID 3HGZ [47,48], according to a new set of criteria [33] as defined in the section of Materials and Methods.
5. a total of 39 (Table 6) interfacial side chain hydrogen bonds were structurally identified for the amylin-IDE complex structure PDB ID 2G48 [45,46], according to a new set of criteria [33] as defined in the section of Materials and Methods.

 doi:10.20944/preprints202402.0063.v1

6. among the 39, 9 (Table 6) interfacial side chain hydrogen bonds were structurally identified at the binding interface of IDE and amylin for the amylin-IDE complex structure PDB ID 2G48 [45,46], according to a new set of criteria [33] as defined in the section of Materials and Methods.
7. a total of 15 (Table 7) interfacial side chain hydrogen bonds were structurally identified for the amylin-IDE complex structure PDB ID 3HGZ [47,48], according to a new set of criteria [33] as defined in the section of Materials and Methods.
8. among the 15, only four (Table 7) interfacial side chain hydrogen bonds were structurally identified at the binding interface of IDE and amylin for the amylin-IDE complex structure PDB ID 3HGZ [47,48], according to a new set of criteria [33] as defined in the section of Materials and Methods.

Table 5. Interfacial salt bridging network analysis within the PDB entries (2G48 [45,46] and 3HGZ [47,48]) according to a new set of criteria [33] as defined in the section of Materials and Methods. In this table, the residue naming scheme is **Chain ID_residue name_residue number**. As defined in the PDB format content of PDB IDs: 2G48 [45,46] and 3HGZ [47,48], chains A and B represent IDE in 3HGZ, chains D and E represent amylin in 3HGZ, while chains A and B represent IDE in 2G48, and chains C and D represent amylin in 2G48, respectively.

PDB ID	Residue A	Atom A	Residue B	Atom B	Distance (Å)
2G48	A_ARG_722	NH1	B_GLU_702	OE2	4.700
2G48	A_ARG_722	NH1	B_ASP_706	OD1	2.987
2G48	A_ARG_722	NH1	B_ASP_706	OD2	2.560
2G48	A_ARG_722	NH2	B_GLU_702	OE1	5.134
2G48	A_ARG_722	NH2	B_GLU_702	OE2	3.255
2G48	A_ARG_722	NH2	B_ASP_706	OD1	4.711
2G48	A_ARG_722	NH2	B_ASP_706	OD2	4.433
2G48	A_LYS_756	NZ	B_GLU_702	OE2	5.525
2G48	A_LYS_756	NZ	B_ASP_706	OD1	3.852
2G48	A_LYS_756	NZ	B_ASP_706	OD2	5.449
2G48	A_LYS_1009	NZ	B_GLU_990	OE1	5.840
2G48	B_ARG_722	NH1	A_ASP_706	OD1	2.728
2G48	B_ARG_722	NH1	A_ASP_706	OD2	3.524
2G48	B_ARG_722	NH2	A_GLU_702	OE1	5.354
2G48	B_ARG_722	NH2	A_ASP_706	OD1	3.653
2G48	B_ARG_722	NH2	A_ASP_706	OD2	5.078
2G48	B_LYS_756	NZ	A_ASP_706	OD1	3.253
2G48	B_LYS_756	NZ	A_ASP_706	OD2	2.575
2G48	B_LYS_1009	NZ	A_GLU_997	OE1	5.095
2G48	C_LYS_1	NZ	A_GLU_341	OE1	3.514
2G48	C_LYS_1	NZ	A_GLU_341	OE2	4.876
2G48	C_LYS_1	NZ	A_GLU_612	OE2	5.297
3HGZ	A_LYS_123	NZ	B_ASP_416	OD1	4.754
3HGZ	A_ARG_164	NH1	B_GLU_408	OE1	3.083
3HGZ	A_ARG_164	NH1	B_GLU_408	OE2	3.662
3HGZ	A_ARG_164	NH2	B_GLU_408	OE1	3.032
3HGZ	A_ARG_164	NH2	B_GLU_408	OE2	4.613
3HGZ	A_LYS_884	NZ	B_GLU_457	OE1	4.680
3HGZ	B_HIS_53	ND1	A_GLU_875	OE1	4.690
3HGZ	B_HIS_53	NE2	A_GLU_875	OE1	4.274
3HGZ	B_LYS_327	NZ	A_GLU_880	OE1	3.476
3HGZ	B_LYS_327	NZ	A_GLU_880	OE2	5.083
3HGZ	B_LYS_415	NZ	A_GLU_133	OE1	5.186
3HGZ	D_LYS_1	NZ	A_GLU_341	OE1	2.441
3HGZ	D_LYS_1	NZ	A_GLU_341	OE2	4.468
3HGZ	E_LYS_1	NZ	B_GLU_341	OE1	3.179
3HGZ	E_LYS_1	NZ	B_GLU_341	OE2	5.147

 doi:10.20944/preprints202402.0063.v1

Table 6. 2G48 [45,46]-specific interfacial side chain hydrogen bonding analysis according to a new set of criteria [33] as defined in the section of Materials and Methods. In this table, the residue naming scheme is **Chain ID_residue name_residue number**, $\angle ADH$ represents the angle formed by acceptor (A), donor (D) and hydrogen (H) $(\angle ADH)$. As defined in the PDB format content of PDB IDs: 2G48 [45,46] and 3HGZ [47,48], chains A and B represent IDE in 3HGZ, chains D and E represent amylin in 3HGZ, while chains A and B represent IDE in 2G48, and chains C and D represent amylin in 2G48, respectively.

PDB ID	Acceptor (A)	Donor (D)	Hydrogen (H)	D-A (Å)	H-A (Å)	∠ADH(°)
2G48	NE2, C_HIS_18	NZ, A_LYS_192	HZ3, A_LYS_192	4.89	4.23	44.36
2G48	OD1, C_ASN_14	OG1, A_THR_220	HG1, A_THR_220	3.22	2.28	9.48
2G48	ND2, C_ASN_14	OG1, A_THR_220	HG1, A_THR_220	3.21	2.65	47.15
2G48	OE1, B_GLN_718	NE2, A_HIS_589	HE2, A_HIS_589	4.14	3.18	16.40
2G48	NE2, B_GLN_718	NE2, A_HIS_589	HE2, A_HIS_589	4.55	3.58	13.52
2G48	OG, B_SER_721	NH1, A_ARG_711	HH12, A_ARG_711	4.90	3.97	20.43
2G48	NE2, B_GLN_718	NH2, A_ARG_711	HH21, A_ARG_711	3.92	3.14	33.89
2G48	OG, B_SER_721	NH2, A_ARG_711	HH21, A_ARG_711	4.86	3.92	19.33
2G48	NE2, B_HIS_589	NE2, A_GLN_718	HE22, A_GLN_718	3.40	2.61	32.75
2G48	OD1, B_ASP_706	NH1, A_ARG_722	HH12, A_ARG_722	2.99	2.41	46.66
2G48	OE2, B_GLU_702	NH2, A_ARG_722	HH22, A_ARG_722	3.25	2.43	29.82
2G48	OE1, B_GLU_699	OG, A_SER_761	HG, A_SER_761	3.84	2.92	13.96
2G48	OE2, B_GLU_699	OG, A_SER_761	HG, A_SER_761	2.52	1.67	22.41
2G48	OD2, B_ASP_586	NE2, A_GLN_762	HE22, A_GLN_762	3.64	3.02	45.51
2G48	NE2, B_GLN_770	NE2, A_GLN_770	HE21, A_GLN_770	4.30	3.39	22.59
2G48	OG, D_SER_19	ND2, B_ASN_139	HD22, B_ASN_139	4.49	3.91	48.99
2G48	OD1, D_ASN_14	OG1, B_THR_220	HG1, B_THR_220	3.09	2.14	8.07
2G48	ND2, D_ASN_14	OG1, B_THR_220	HG1, B_THR_220	3.42	2.85	46.81
2G48	OE1, A_GLN_718	NE, B_ARG_711	HE, B_ARG_711	4.89	3.96	20.15
2G48	OG, A_SER_721	NE, B_ARG_711	HE, B_ARG_711	4.94	4.15	34.49
2G48	OG, A_SER_721	NH1, B_ARG_711	HH12, B_ARG_711	4.28	3.36	20.95
2G48	OD1, A_ASP_706	NH1, B_ARG_722	HH12, B_ARG_722	2.73	1.91	29.32
2G48	OD2, A_ASP_706	NH1, B_ARG_722	HH12, B_ARG_722	3.52	2.69	29.77
2G48	OD1, A_ASP_706	NH2, B_ARG_722	HH21, B_ARG_722	3.65	3.09	49.48
2G48	OD2, A_ASP_706	NZ, B_LYS_756	HZ1, B_LYS_756	2.57	1.59	10.38
2G48	OE1, A_GLU_699	OG, B_SER_761	HG, B_SER_761	4.00	3.07	11.68
2G48	OE2, A_GLU_699	OG, B_SER_761	HG, B_SER_761	2.51	1.64	19.94
2G48	OD2, A_ASP_586	NE2, B_GLN_762	HE22, B_GLN_762	4.17	3.60	49.58
2G48	NE2, A_GLN_770	NE2, B_GLN_770	HE21, B_GLN_770	4.30	3.46	30.40
2G48	OD1, D_ASN_22	NH2, B_ARG_847	HH22, B_ARG_847	4.10	3.14	17.00
2G48	ND2, D_ASN_22	NH2, B_ARG_847	HH22, B_ARG_847	4.95	3.97	13.60
2G48	OE1, A_GLU_341	NZ, C_LYS_1	HZ3, C_LYS_1	3.51	2.72	32.95
2G48	OE2, A_GLU_341	NZ, C_LYS_1	HZ3, C_LYS_1	4.88	4.20	43.27
2G48	ND1, A_HIS_332	OG1, C_THR_4	HG1, C_THR_4	3.10	2.41	37.40
2G48	OG1, A_THR_220	ND2, C_ASN_14	HD22, C_ASN_14	3.21	2.37	28.58
2G48	NE2, A_HIS_679	NE2, C_HIS_18	HE2, C_HIS_18	4.27	3.60	43.28
2G48	OG1, B_THR_220	ND2, D_ASN_14	HD22, D_ASN_14	3.42	2.67	36.00
2G48	NE2, B_HIS_679	NE2, D_HIS_18	HE2, D_HIS_18	4.32	3.75	49.86

Table 7. 3HGZ [47,48]-specific interfacial side chain hydrogen bonding analysis according to a new set of criteria [33] as defined in the section of Materials and Methods. In this table, the residue naming scheme is **Chain ID_residue name_residue number**, $\angle ADH$ represents the angle formed by acceptor (A), donor (D) and hydrogen (H) $(\angle ADH)$. As defined in the PDB format content of PDB IDs: 2G48 [45,46] and 3HGZ [47,48], chains A and B represent IDE in 3HGZ, chains D and E represent amylin in 3HGZ, while chains A and B represent IDE in 2G48, and chains C and D represent amylin in 2G48, respectively.

PDB ID	Acceptor (A)	Donor (D)	Hydrogen (H)	D-A (Å)	H-A (Å)	∠ADH(°)
3HGZ	NE2, B_GLN_407	NZ, A_LYS_120	HZ3, A_LYS_120	4.83	4.00	31.04
3HGZ	OE1, B_GLU_408	NH1, A_ARG_164	HH11, A_ARG_164	3.08	2.20	24.18
3HGZ	OE2, B_GLU_408	NH1, A_ARG_164	HH11, A_ARG_164	3.66	2.70	14.52
3HGZ	OE1, B_GLU_408	NH2, A_ARG_164	HH21, A_ARG_164	3.03	2.13	21.99
3HGZ	OE2, B_GLU_408	NH2, A_ARG_164	HH21, A_ARG_164	4.61	3.89	39.58
3HGZ	OE1, B_GLN_412	NH2, A_ARG_164	HH22, A_ARG_164	3.72	2.94	34.36
3HGZ	OE1, B_GLU_457	OG1, A_THR_878	HG1, A_THR_878	2.79	2.15	40.71
3HGZ	OE2, B_GLU_457	OG1, A_THR_878	HG1, A_THR_878	3.07	2.47	43.72
3HGZ	OE1, B_GLU_457	NZ, A_LYS_884	HZ3, A_LYS_884	4.68	3.74	18.88
3HGZ	OG1, B_THR_55	NZ, A_LYS_933	HZ2, A_LYS_933	3.39	2.77	44.49
3HGZ	OE1, A_GLU_880	NZ, B_LYS_327	HZ1, B_LYS_327	3.48	2.53	17.30
3HGZ	OE1, A_GLU_341	NZ, D_LYS_1	HZ1, D_LYS_1	2.44	1.85	44.11
3HGZ	OH, A_TYR_609	NZ, D_LYS_1	HZ2, D_LYS_1	3.91	3.25	43.14
3HGZ	OE1, B_GLU_341	NZ, E_LYS_1	HZ2, E_LYS_1	3.18	2.42	34.86
3HGZ	OH, B_TYR_609	NZ, E_LYS_1	HZ3, E_LYS_1	3.97	3.23	37.37

 doi:10.20944/preprints202402.0063.v1

4.2. Structural identification of an electrostatic hotspot at amylin-IDE binding interface

Among the residue-specific electrostatic interactions at the amylin-IDE binding interface described above, one extraordinary pair of oppositely charged residues appear rather outstanding: lysine (Lys1, K1) residue of amylin and Glu341 (E341) of IDE, as this residue pair is the only one where interfacial electrostatic interactions were structurally identified at the amylin-IDE binding interface for two experimental structures representing the amylin-IDE complex, with PDB IDs: 2G48 [45,46] and 3HGZ [47,48] as listed in Table 1.

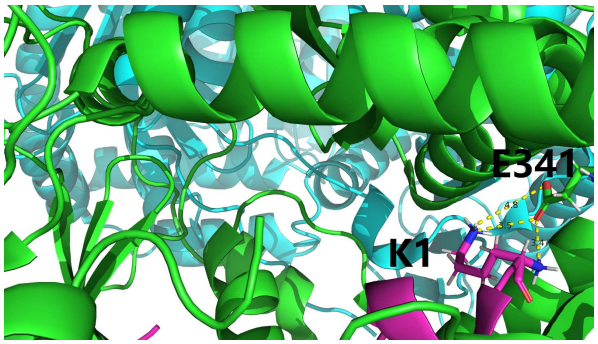

Figure 2. Two sets of interfacial salt bridges (dotted yellow sticks) between Lys1 (K1) of amylin and Glu341 (E341) of IDE. This figure is prepared by PyMol [53] with PDB ID 2G48 [45,46]. In this figure, the color scheme is the same as in Figure 1.

Take 2G48 [45,46] for example, one 3.514 Å interfacial salt bridge (Figureřefpymol2) was found to be formed between the oppositely charged side chains of Lys1 of amylin and Glu341 of IDE, while two interfacial salt bridges (2.441 and 3.179 Å) were also found to be formed between the oppositely charged side chains of Lys1 of amylin and Glu341 of IDE for 3HGZ [47,48]. Moreover, while no further salt bridges were found to be formed according to the old set of criteria as defined in [33], they are still quite close to each other for the side chains of Lys1 of amylin and Glu341 of IDE. Take 2G48 [45,46] for example, apart from the salt bridge, other positively charged side chain atoms of Lys1 of amylin are only 4.876 and 5.297 Å away from the negatively charged side chain oxygens of Glu341 of IDE, as shown in Figuresřefpymol2 and 3.

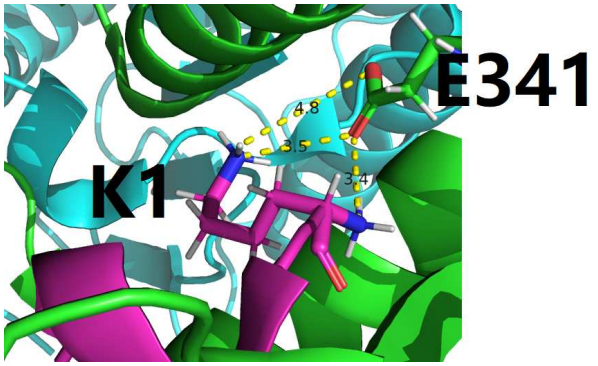

Figure 3. A closer (than Figureřefpymol2) view of two sets of interfacial salt bridges (dotted yellow sticks) between Lys1 (K1) of amylin and Glu341 (E341) of IDE. This figure is prepared by PyMol [53] with PDB ID 2G48 [45,46]. In this figure, the color scheme is the same as in Figure 1.

In addition to interfacial salt bridges, the one extraordinary pair, i.e., Lys1 of amylin and Glu341 of IDE, were also found to be involved in a set of interfacial side chain hydrogen bonds, as shown by two yellow rows in Table 7 and also two yellow rows in Table 6, according to a new set of criteria [33] as defined in the section of Materials and Methods. Finally, what even more interesting is one interfacial side chain bridges formed between Lys1 of amylin and Glu341 of IDE, as shown in Figuresřefpymol2

 doi:10.20944/preprints202402.0063.v1

and 3, the main chain amide nitrogen (positively charged) of Lys1 of amylin is only 3.4 Å away from the negatively charged side chain oxygen of Glu341 of IDE, making the residue pair close to each other enough to form a strong main chain-side chain interfacial salt bridge, further strengthening the binding between amylin and IDE.

Taken together, these three sets of interfacial electrostatic interactions between Lys1 of amylin and Glu341 of IDE, i.e., side chain-side chain interfacial salt bridges, side chain-side chain interfacial hydrogen bonds, main chain-side chain interfacial salt bridges, highlights an extraordinary electrostatic hotspot at the amylin-IDE binding interface, making it an attractive precise target for small molecule inhibitor to reach inside IDE (the cage, Figureřefpymol1) and disrupt the amylin-IDE interaction for improved metabolic homeostasis.

5. Conclusion

Starting from two experimental structures representing the amylin-IDE complex, with PDB IDs: 2G48 [45,46] and 3HGZ [47,48] as listed in Table 1, this article puts forward a set of structural characterization for residue-specific electrostatic interactions at the amylin-IDE binding interface, as listed in Tables 2, 3, 4, 5, 6 and 7. Moreover, this article also highlights one intriguing electrostatic hotspot (Figuresřefpymol2 and 3) between the first N-terminal lysine (Lys1, K1) residue of amylin and Glu341 (E341) of IDE, with both interfacial salt bridges and side chain hydrogen bonds formed between the two oppositely charged residues sitting at the binding interface of amylin-IDE.

To sum up,

1. the structural identification of electrostatic hotspots at the binding interface of amylin and IDE presents a promising avenue for the development of small molecules capable of disrupting this crucial interaction [54–56].
2. This finding also contributes to the growing body of knowledge aimed at unraveling the intricacies of protein–protein interactions and provides a foundation for future research endeavors in the development of targeted therapeutics for metabolic disorders, particularly diabetes (T2DM) and obesity [57,58].
3. The rationale for targeting electrostatic hotspots in the amylin-IDE interaction lies in the role of such sites as preferred binding locations for drug-like small molecules. By pinpointing these hotspots, we aim to provide a precise target for the development of small molecules capable of disrupting the amylin-IDE interaction. The potential therapeutic implications of such disruptors extend to modulating glucose homeostasis and mitigating the risk of amyloid formation, which is particularly relevant in the context of type 2 diabetes.

6. Discussion

6.1. Disrupting the amylin-IDE interaction: a drug discovery and design perspective

In drug discovery and design, targeting the interaction between amylin and IDE could be a potential strategy for therapeutic intervention. As amylin is involved in the regulation of blood glucose levels, manipulating its interaction with IDE might be explored as a way to modulate glucose homeostasis. While this article identified an intriguing electrostatic hotspots at the amylin-IDE binding interface, offering precise targets for therapeutic intervention and the development of small molecule inhibitors targeting the amylin-IDE interaction, the inhibition of the interaction between amylin and IDE can also lead to side effects such as glucose intolerance [59], as the intricate interplay between amylin and IDE constitutes a pivotal aspect of glucose homeostasis, with implications for the prevention of amyloid formation and maintenance of metabolic health [60–62]. Moreover, disrupting the interaction between amylin and IDE could have unintended consequences, as IDE is involved in the degradation of various peptides, and altering its interaction with amylin might affect the levels of other important regulatory molecules, selectivity is a key challenge in the design of small molecule

 doi:10.20944/preprints202402.0063.v1

inhibitor or even other molecular modalities such as small peptide of peptide-small molecule conjugate. Finally, still essential is a thorough understanding of the biological consequences of disrupting the amylin-IDE interaction, while disrupting the interaction between amylin and IDE could be a potential avenue for drug development, especially in the context of diabetes, obesity or even neurodegenerative diseases.

6.2. High-throughput comprehensive structural biophysical analysis: a methological perspective

In 2017, a comprehensive structural biophysical (CSB) approach was for the first time used in the analysis of experimental complex structures deposited in PDB [31] to address this question: how do SMA-linked mutations of *SMN1* lead to structural/functional deficiency of the SMA protein i.e., the survivor motor neuron protein [33]? Here, the same structural biophysical approach was used here for the analysis of experimental complex structures of amylin and IDE, allowing for the precise identification of electrostatic hotspots at the binding interface of amylin and insulin-degrading enzyme. This level of precision aids in targeting specific regions for the development of small molecules. Moreover, By exploring the structural details and biophysical characteristics of the interaction, this approach provides valuable insights into the molecular interactions between amylin and insulin-degrading enzyme. Understanding these interactions is crucial for rational design of effective small molecule disruptors with high specificity, i.e., without affecting other biological processes. This specificity is crucial for minimizing off-target effects and enhancing the safety profile of potential therapeutic agents.

In addition, the information obtained through this approach contributes to rational drug design by providing a solid foundation for the development of small molecules. The identified hotspots serve as rational targets for disrupting the interaction, potentially enhancing the success rate of drug development efforts. Furthermore, in light of the increasingly large size of the Protein Data Bank, this CSB approach technically is applicable for a exhaustive analysis of the entire PDB for high-throughput extraction of structural and biophysical features [63,64] and continued generation and accumulation of synthetic structural and biophysical data with reasonable accuracy to support the development of machine learning-models such as GIBAC [65]. With this respect, however, in original PDB-format data, the experimentally determined atomic coordinates are presented in the ATOM records, and chances are that they do not exactly match the sequence (consisting of nucleic and/or amino acid residues) of the experimental sample *per se*, be it protein, DNA, RNA or their complexes with drugs and/or other small molecules [66,67].

Take amylin and IDE for example, the fasta format sequence of amylin in PDB ID 2G48 [45,46] is as below:

>2G48_2 | Chains C, D | Islet amyloid polypeptide | null [45,46]
KCNTATCATQRLANFLVHSSNNFGAILSSTNVGSNTY
while the fasta format sequence of amylin in PDB ID 3HGZ [47,48] is as below:
>3HGZ_2 | Chains C[auth D], D[auth E] | Islet amyloid polypeptide | null (9606) [47,48]
KCNTATCATQRLANFLVHSSNNFGAILSSTNVGSNTY

As listed in Table 8, in PDB ID 2G48 [45,46], there are a total of 37 residues for amylin in the experimental sample, with atomic coordinate information of 19 missing for chain C (amylin in PDB ID 2G48) and 20 missing for chain D (amylin in PDB ID 2G48), while in PDB ID 3HGZ [47,48], there are also a total of 37 residues for amylin in the experimental sample, with atomic coordinate information of 30 missing for chain D (amylin in PDB ID 3HGZ) and 27 missing for chain D (amylin in PDB ID 3HGZ).

 doi:10.20944/preprints202402.0063.v1

Table 8. Experimentally uncharted territories (EUTs) in two structural models representing IDE-amylin complex, as described by REMARK 465 in the PDB format content of PDB IDs: 2G48 [45,46] and 3HGZ [47,48].

PDB ID	REMARK	REMARK ID	ResName	Chain ID	ResID
3HGZ	REMARK	465	ASN	D	3
3HGZ	REMARK	465	THR	D	4
3HGZ	REMARK	465	ALA	D	5
3HGZ	REMARK	465	THR	D	6
3HGZ	REMARK	465	CYS	D	7
3HGZ	REMARK	465	ALA	D	8
3HGZ	REMARK	465	THR	D	9
3HGZ	REMARK	465	GLN	D	10
3HGZ	REMARK	465	ARG	D	11
3HGZ	REMARK	465	VAL	D	17
3HGZ	REMARK	465	HIS	D	18
3HGZ	REMARK	465	SER	D	19
3HGZ	REMARK	465	SER	D	20
3HGZ	REMARK	465	ASN	D	21
3HGZ	REMARK	465	ASN	D	22
3HGZ	REMARK	465	PHE	D	23
3HGZ	REMARK	465	GLY	D	24
3HGZ	REMARK	465	ALA	D	25
3HGZ	REMARK	465	ILE	D	26
3HGZ	REMARK	465	LEU	D	27
3HGZ	REMARK	465	SER	D	28
3HGZ	REMARK	465	SER	D	29
3HGZ	REMARK	465	THR	D	30
3HGZ	REMARK	465	ASN	D	31
3HGZ	REMARK	465	VAL	D	32
3HGZ	REMARK	465	GLY	D	33
3HGZ	REMARK	465	SER	D	34
3HGZ	REMARK	465	ASN	D	35
3HGZ	REMARK	465	THR	D	36
3HGZ	REMARK	465	TYR	D	37
3HGZ	REMARK	465	THR	E	4
3HGZ	REMARK	465	ALA	E	5
3HGZ	REMARK	465	THR	E	6
3HGZ	REMARK	465	THR	E	9
3HGZ	REMARK	465	GLN	E	10
3HGZ	REMARK	465	ARG	E	11
3HGZ	REMARK	465	VAL	E	17
3HGZ	REMARK	465	HIS	E	18
3HGZ	REMARK	465	SER	E	19
3HGZ	REMARK	465	SER	E	20
3HGZ	REMARK	465	ASN	E	21
3HGZ	REMARK	465	ASN	E	22
3HGZ	REMARK	465	PHE	E	23
3HGZ	REMARK	465	GLY	E	24
3HGZ	REMARK	465	ALA	E	25
3HGZ	REMARK	465	ILE	E	26
3HGZ	REMARK	465	LEU	E	27
3HGZ	REMARK	465	SER	E	28
3HGZ	REMARK	465	SER	E	29
3HGZ	REMARK	465	THR	E	30
3HGZ	REMARK	465	ASN	E	31
3HGZ	REMARK	465	VAL	E	32
3HGZ	REMARK	465	GLY	E	33
3HGZ	REMARK	465	SER	E	34
3HGZ	REMARK	465	ASN	E	35
3HGZ	REMARK	465	THR	E	36
3HGZ	REMARK	465	TYR	E	37
2G48	REMARK	465	CYS	C	7
2G48	REMARK	465	ALA	C	8
2G48	REMARK	465	THR	C	9
2G48	REMARK	465	ASN	C	22
2G48	REMARK	465	PHE	C	23
2G48	REMARK	465	GLY	C	24
2G48	REMARK	465	ALA	C	25
2G48	REMARK	465	ILE	C	26
2G48	REMARK	465	LEU	C	27
2G48	REMARK	465	SER	C	28
2G48	REMARK	465	SER	C	29
2G48	REMARK	465	THR	C	30
2G48	REMARK	465	ASN	C	31
2G48	REMARK	465	VAL	C	32
2G48	REMARK	465	GLY	C	33
2G48	REMARK	465	SER	C	34
2G48	REMARK	465	ASN	C	35
2G48	REMARK	465	THR	C	36
2G48	REMARK	465	TYR	C	37
2G48	REMARK	465	ALA	D	5
2G48	REMARK	465	THR	D	6
2G48	REMARK	465	CYS	D	7
2G48	REMARK	465	ALA	D	8
2G48	REMARK	465	THR	D	9
2G48	REMARK	465	GLN	D	10
2G48	REMARK	465	GLY	D	24
2G48	REMARK	465	ALA	D	25
2G48	REMARK	465	ILE	D	26
2G48	REMARK	465	LEU	D	27
2G48	REMARK	465	SER	D	28
2G48	REMARK	465	SER	D	29
2G48	REMARK	465	THR	D	30
2G48	REMARK	465	ASN	D	31
2G48	REMARK	465	VAL	D	32
2G48	REMARK	465	GLY	D	33
2G48	REMARK	465	SER	D	34
2G48	REMARK	465	ASN	D	35
2G48	REMARK	465	THR	D	36
2G48	REMARK	465	TYR	D	37

 doi:10.20944/preprints202402.0063.v1

As previously described in [68] in 2017, the past 53 years of experimental structure deposition in PDB also saw continued accumulation of experimentally uncharted territories (EUTs) inside it, reaching a point already where it is increasingly pressing for biomolecular structures (especially membrane proteins like Ca^{2+} channel [69,70]) to be experimentally determined in an EUT-less manner, as exemplified here again by the experimentally uncharted territories (EUTs) in two structural models representing IDE-amylin complex (PDB IDs: 2G48 [45,46] and 3HGZ [47,48]).

7. Ethical statement

No ethical approval is required.

8. Declaration of generative AI and AI-assisted technologies in the writing process

During the preparation of this work, the author used OpenAI's ChatGPT in order to improve the readability of the manuscript, and to make it as concise and short as possible. After using this tool, the author reviewed and edited the content as needed and takes full responsibility for the content of the publication.

Author Contributions: Conceptualization, W.L.; methodology, W.L.; software, W.L.; validation, W.L.; formal analysis, W.L.; investigation, W.L.; resources, W.L.; data duration, W.L.; writing–original draft preparation, W.L.; writing–review and editing, W.L.; visualization, W.L.; supervision, W.L.; project administration, W.L.; funding acquisition, not applicable.

Funding: This research received no external funding.

Conflicts of Interest: The author declares no conflict of interest.

References

1. Mathiesen, D.S.; Bagger, J.I.; Knop, F.K. Long-acting amylin analogues for the management of obesity. *Current Opinion in Endocrinology, Diabetes & Obesity* **2022**, *29*, 183–190. doi:10.1097/med.0000000000000716.
2. Hay, D.L.; Chen, S.; Lutz, T.A.; Parkes, D.G.; Roth, J.D. Amylin: Pharmacology, Physiology, and Clinical Potential. *Pharmacological Reviews* **2015**, *67*, 564–600. doi:10.1124/pr.115.010629.
3. Alghrably, M.; Czaban, I.; Jaremko, L.; Jaremko, M. Interaction of amylin species with transition metals and membranes. *Journal of Inorganic Biochemistry* **2019**, *191*, 69–76. doi:10.1016/j.jinorgbio.2018.11.004.
4. Moracci, L.; Crotti, S.; Traldi, P.; Agostini, M.; Cosma, C.; Lapolla, A. Role of mass spectrometry in the study of interactions between amylin and metal ions. *Mass Spectrometry Reviews* **2021**, *42*, 984–1007. doi:10.1002/mas.21732.
5. Bennett, R.G.; Duckworth, W.C.; Hamel, F.G. Degradation of Amylin by Insulin-degrading Enzyme. *Journal of Biological Chemistry* **2000**, *275*, 36621–36625. doi:10.1074/jbc.m006170200.
6. Tang, W.J. Targeting Insulin-Degrading Enzyme to Treat Type 2 Diabetes Mellitus. *Trends in Endocrinology & Metabolism* **2016**, *27*, 24–34. doi:10.1016/j.tem.2015.11.003.
7. Adamek, R.N.; Suire, C.N.; Stokes, R.W.; Brizuela, M.K.; Cohen, S.M.; Leissring, M.A. Hydroxypyridinethione Inhibitors of Human Insulin-Degrading Enzyme. *ChemMedChem* **2021**, *16*, 1776–1788. doi:10.1002/cmdc.202100111.
8. Ling, W.; Huang, Y.M.; Qiao, Y.C.; Zhang, X.X.; Zhao, H.L. Human Amylin: From Pathology to Physiology and Pharmacology. *Current Protein & Peptide Science* **2019**, *20*, 944–957. doi:10.2174/1389203720666190328111833.
9. Yang, Y.; Song, W. Molecular links between Alzheimer's disease and diabetes mellitus. *Neuroscience* **2013**, *250*, 140–150. doi:10.1016/j.neuroscience.2013.07.009.
10. Sousa, L.; Guarda, M.; Meneses, M.J.; Macedo, M.P.; Vicente Miranda, H. Insulin-degrading enzyme: an ally against metabolic and neurodegenerative diseases. *The Journal of Pathology* **2021**, *255*, 346–361. doi:10.1002/path.5777.
11. Tundo, G.R.; Sbardella, D.; Ciaccio, C.; Grasso, G.; Gioia, M.; Coletta, A.; Polticelli, F.; Di Pierro, D.; Milardi, D.; Van Endert, P.; Marini, S.; Coletta, M. Multiple functions of insulin-degrading

enzyme: a metabolic crosslight? *Critical Reviews in Biochemistry and Molecular Biology* **2017**, *52*, 554–582. doi:10.1080/10409238.2017.1337707.

12. Sharma, S.K.; Chorell, E.; Wittung-Stafshede, P. Insulin-degrading enzyme is activated by the C-terminus of α-synuclein. *Biochemical and Biophysical Research Communications* **2015**, *466*, 192–195. doi:10.1016/j.bbrc.2015.09.002.
13. Elseweidy, M.M.; Amin, R.S.; Atteia, H.H.; Ali, M.A. Vitamin D3 intake as regulator of insulin degrading enzyme and insulin receptor phosphorylation in diabetic rats. *Biomedicine & Pharmacotherapy* **2017**, *85*, 155–159. doi:10.1016/j.biopha.2016.11.116.
14. Maianti, J.P.; McFedries, A.; Foda, Z.H.; Kleiner, R.E.; Du, X.Q.; Leissring, M.A.; Tang, W.J.; Charron, M.J.; Seeliger, M.A.; Saghatelian, A.; Liu, D.R. Anti-diabetic activity of insulin-degrading enzyme inhibitors mediated by multiple hormones. *Nature* **2014**, *511*, 94–98. doi:10.1038/nature13297.
15. Guo, Q.; Manolopoulou, M.; Bian, Y.; Schilling, A.B.; Tang, W.J. Molecular Basis for the Recognition and Cleavages of IGF-II, TGF-α, and Amylin by Human Insulin-Degrading Enzyme. *Journal of Molecular Biology* **2010**, *395*, 430–443. doi:10.1016/j.jmb.2009.10.072.
16. Schilling, M.A. Unraveling Alzheimer's: Making Sense of the Relationship between Diabetes and Alzheimer's Disease1. *Journal of Alzheimer's Disease* **2016**, *51*, 961–977. doi:10.3233/jad-150980.
17. Bennett, R.G.; Hamel, F.G.; Duckworth, W.C. An Insulin-Degrading Enzyme Inhibitor Decreases Amylin Degradation, Increases Amylin-Induced Cytotoxicity, and Increases Amyloid Formation in Insulinoma Cell Cultures. *Diabetes* **2003**, *52*, 2315–2320. doi:10.2337/diabetes.52.9.2315.
18. QIU, W.; FOLSTEIN, M. Insulin, insulin-degrading enzyme and amyloid-β peptide in Alzheimer's disease: review and hypothesis. *Neurobiology of Aging* **2006**, *27*, 190–198. doi:10.1016/j.neurobiolaging.2005.01.004.
19. Durham, T.B.; Toth, J.L.; Klimkowski, V.J.; Cao, J.X.; Siesky, A.M.; Alexander-Chacko, J.; Wu, G.Y.; Dixon, J.T.; McGee, J.E.; Wang, Y.; Guo, S.Y.; Cavitt, R.N.; Schindler, J.; Thibodeaux, S.J.; Calvert, N.A.; Coghlan, M.J.; Sindelar, D.K.; Christe, M.; Kiselyov, V.V.; Michael, M.D.; Sloop, K.W. Dual Exosite-binding Inhibitors of Insulin-degrading Enzyme Challenge Its Role as the Primary Mediator of Insulin Clearance in Vivo. *Journal of Biological Chemistry* **2015**, *290*, 20044–20059. doi:10.1074/jbc.m115.638205.
20. Song, E.S.; Ozbil, M.; Zhang, T.; Sheetz, M.; Lee, D.; Tran, D.; Li, S.; Prabhakar, R.; Hersh, L.B.; Rodgers, D.W. An Extended Polyanion Activation Surface in Insulin Degrading Enzyme. *PLOS ONE* **2015**, *10*, e0133114. doi:10.1371/journal.pone.0133114.
21. Costes, S.; Butler, P. Insulin-Degrading Enzyme Inhibition, a Novel Therapy for Type 2 Diabetes? *Cell Metabolism* **2014**, *20*, 201–203. doi:10.1016/j.cmet.2014.07.016.
22. Bellia, F.; Grasso, G. The role of copper(II) and zinc(II) in the degradation of human and murine IAPP by insulin-degrading enzyme: Metal ion modulation of IAPP degradation by IDE. *Journal of Mass Spectrometry* **2014**, *49*, 274–279. doi:10.1002/jms.3338.
23. Zhang, Y.; Yin, F.; Liu, J.; Wang, Y. Geniposide protects pancreatic INS-1E β cells from hIAPP-induced cell damage: Potential involvement of insulin degrading-enzyme. *Cell Biology International* **2014**, *39*, 373–378. doi:10.1002/cbin.10394.
24. Suire, C.N.; Brizuela, M.K.; Leissring, M.A. Quantitative, High-Throughput Assays for Proteolytic Degradation of Amylin. *Methods and Protocols* **2020**, *3*, 81. doi:10.3390/mps3040081.
25. Hogan, M.F.; Meier, D.T.; Zraika, S.; Templin, A.T.; Mellati, M.; Hull, R.L.; Leissring, M.A.; Kahn, S.E. Inhibition of Insulin-Degrading Enzyme Does Not Increase Islet Amyloid Deposition in Vitro. *Endocrinology* **2016**, *157*, 3462–3468. doi:10.1210/en.2016-1410.
26. Song, E.S.; Jang, H.; Guo, H.F.; Juliano, M.A.; Juliano, L.; Morris, A.J.; Galperin, E.; Rodgers, D.W.; Hersh, L.B. Inositol phosphates and phosphoinositides activate insulin-degrading enzyme, while phosphoinositides also mediate binding to endosomes. *Proceedings of the National Academy of Sciences* **2017**, *114*. doi:10.1073/pnas.1613447114.
27. Liu, Z.; Zhu, H.; Fang, G.G.; Walsh, K.; Mwamburi, M.; Wolozin, B.; Abdul-Hay, S.O.; Ikezu, T.; Leissring, M.A.; Qiu, W.Q. Characterization of Insulin Degrading Enzyme and Other Amyloid-β Degrading Proteases in Human Serum: A Role in Alzheimer's Disease? *Journal of Alzheimer's Disease* **2012**, *29*, 329–340. doi:10.3233/jad-2011-111472.
28. Shen, Y.; Joachimiak, A.; Rich Rosner, M.; Tang, W.J. Structures of human insulin-degrading enzyme reveal a new substrate recognition mechanism. *Nature* **2006**, *443*, 870–874. doi:10.1038/nature05143.

29. Bailey, C.J. Drugs on the horizon for diabesity. *Current Diabetes Reports* **2005**, *5*, 353–359. doi:10.1007/s11892-005-0093-1.
30. Fernandez-Gamba, A.; Leal, M.; Morelli, L.; Castano, E. Insulin-Degrading Enzyme: Structure-Function Relationship and its Possible Roles in Health and Disease. *Current Pharmaceutical Design* **2009**, *15*, 3644–3655. doi:10.2174/138161209789271799.
31. Berman, H.; Henrick, K.; Nakamura, H. Announcing the worldwide Protein Data Bank. *Nature Structural & Molecular Biology* **2003**, *10*, 980–980.
32. Li, W. Half-a-century Burial of ρ, ϑ and φ in PDB. *Preprint* **2021**.
33. Li, W. How do SMA-linked mutations of *SMN1* lead to structural/functional deficiency of the SMA protein? *PLOS ONE* **2017**, *12*, e0178519.
34. Li, W. Delving deep into the structural aspects of a furin cleavage site inserted into the spike protein of SARS-CoV-2: A structural biophysical perspective. *Biophysical Chemistry* **2020**, *264*, 106420.
35. Kortemme, T.; Kim, D.E.; Baker, D. Computational Alanine Scanning of Protein-Protein Interfaces. *Science Signaling* **2004**, *2004*, pl2–pl2.
36. Li, W. How Structural Modifications of Insulin Icodec Contributes to Its Prolonged Duration of Action: A Structural and Biophysical Perspective **2023**. doi:10.20944/preprints202311.1048.v1.
37. Li, Y.; Liang, Z.; Tian, Y.; Cai, W.; Weng, Z.; Chen, L.; Zhang, H.; Bao, Y.; Zheng, H.; Zeng, S.; Bei, C.; Li, Y. High-affinity PD-1 molecules deliver improved interaction with PD-L1 and PD-L2. *Cancer Science* **2018**, *109*, 2435–2445.
38. Li, W. Delving Deep into the Structural Aspects of the BPro28-BLys29 Exchange in Insulin Lispro: A Structural Biophysical Lesson **2020**.
39. Li, W. Extracting the Interfacial Electrostatic Features from Experimentally Determined Antigen and/or Antibody-Related Structures inside Protein Data Bank for Machine Learning-Based Antibody Design **2020**. doi:10.20944/preprints202003.0011.v1.
40. Wong, S.K.; Li, W.; Moore, M.J.; Choe, H.; Farzan, M. A 193-Amino Acid Fragment of the SARS Coronavirus S Protein Efficiently Binds Angiotensin-converting Enzyme 2. *Journal of Biological Chemistry* **2003**, *279*, 3197–3201.
41. Ho, M.W.; O'Brien, J.S. Gaucher's Disease: deficiency of CID β-Glucosidase and Reconstitution of Enzyme Activity In Vitro. *Proc. Natl. Acad. Sci. USA* **1971**, *68*, 2810–2813.
42. Abraham, E.P.; Chain, E. An enzyme from bacteria able to destroy penicillin. *Nature* **1940**, *146*, 837–837.
43. Li, W. Strengthening Semaglutide-GLP-1R Binding Affinity Via a Val27-Arg28 Exchange in the Peptide Backbone of Semaglutide: A Computational Structural Approach. *Journal of Computational Biophysics and Chemistry* **2021**, pp. 1–5.
44. Li, W. Designing rt-PA Analogs to Release its Trapped Thrombolytic Activity. *Journal of Computational Biophysics and Chemistry* **2021**, *20*, 719–727.
45. Shen, Y.; Joachimiak, A.; Rich Rosner, M.; Tang, W.J. Structures of human insulin-degrading enzyme reveal a new substrate recognition mechanism. *Nature* **2006**, *443*, 870–874. doi:10.1038/nature05143.
46. Shen, Y.; Tang, W.J. crystal structure of human insulin-degrading enzyme in complex with amylin, 2006. doi:10.2210/pdb2g48/pdb.
47. Guo, Q.; Bian, Y.; Tang, W. Crystal structure of human insulin-degrading enzyme in complex with amylin, 2009. doi:10.2210/pdb3hgz/pdb.
48. Guo, Q.; Manolopoulou, M.; Bian, Y.; Schilling, A.B.; Tang, W.J. Molecular Basis for the Recognition and Cleavages of IGF-II, TGF-α, and Amylin by Human Insulin-Degrading Enzyme. *Journal of Molecular Biology* **2010**, *395*, 430–443. doi:10.1016/j.jmb.2009.10.072.
49. Pettersen, E.F.; Goddard, T.D.; Huang, C.C.; Couch, G.S.; Greenblatt, D.M.; Meng, E.C.; Ferrin, T.E. UCSF Chimera: A visualization system for exploratory research and analysis. *Journal of Computational Chemistry* **2004**, *25*, 1605–1612.
50. Yuan, Y.; Cao, D.; Zhang, Y.; Ma, J.; Qi, J.; Wang, Q.; Lu, G.; Wu, Y.; Yan, J.; Shi, Y.; Zhang, X.; Gao, G.F. Cryo-EM structures of MERS-CoV and SARS-CoV spike glycoproteins reveal the dynamic receptor binding domains. *Nature Communications* **2017**, *8*.
51. Li, W. Structural and Functional Consequences of the SMA-Linked Missense Mutations of the Survival Motor Neuron Protein: A Brief Update. In *Novel Aspects on Motor Neuron Disease*; IntechOpen, 2019.

52. Deciphering critical amino acid residues to modify and enhance the binding affinity of ankyrin scaffold specific to capsid protein of human immunodeficiency virus type 1. *Asian Pacific Journal of Allergy and Immunology* **2017**.
53. DeLano, W.L. Pymol: An open-source molecular graphics tool. *CCP4 Newsletter On Protein Crystallography* **2002**, *40*, 82–92.
54. Marmentini, C.; Guimarães, D.S.P.; de Lima, T.I.; Teófilo, F.B.S.; da Silva, N.S.; Soares, G.M.; Boschero, A.C.; Kurauti, M.A. Rosiglitazone protects INS-1E cells from human islet amyloid polypeptide toxicity. *European Journal of Pharmacology* **2022**, *928*, 175122. doi:10.1016/j.ejphar.2022.175122.
55. Qiu, W.Q.; Zhu, H. Amylin and its analogs: a friend or foe for the treatment of Alzheimer's disease? *Frontiers in Aging Neuroscience* **2014**, *6*. doi:10.3389/fnagi.2014.00186.
56. Li, P.; Kuo, W.L.; Yousef, M.; Rosner, M.R.; Tang, W.J. The C-terminal domain of human insulin degrading enzyme is required for dimerization and substrate recognition. *Biochemical and Biophysical Research Communications* **2006**, *343*, 1032–1037. doi:10.1016/j.bbrc.2006.03.083.
57. Lam, V.K.L.; Ma, R.C.W.; Lee, H.M.; Hu, C.; Park, K.S.; Furuta, H.; Wang, Y.; Tam, C.H.T.; Sim, X.; Ng, D.P.K.; Liu, J.; Wong, T.Y.; Tai, E.S.; Morris, A.P.; Tang, N.L.S.; Woo, J.; Leung, P.C.; Kong, A.P.S.; Ozaki, R.; Jia, W.P.; Lee, H.K.; Nanjo, K.; Xu, G.; Ng, M.C.Y.; So, W.Y.; Chan, J.C.N. Genetic Associations of Type 2 Diabetes with Islet Amyloid Polypeptide Processing and Degrading Pathways in Asian Populations. *PLoS ONE* **2013**, *8*, e62378. doi:10.1371/journal.pone.0062378.
58. Aston-Mourney, K.; Zraika, S.; Udayasankar, J.; Subramanian, S.L.; Green, P.S.; Kahn, S.E.; Hull, R.L. Matrix Metalloproteinase-9 Reduces Islet Amyloid Formation by Degrading Islet Amyloid Polypeptide. *Journal of Biological Chemistry* **2013**, *288*, 3553–3559. doi:10.1074/jbc.m112.438457.
59. Tang, W.J. Targeting Insulin-Degrading Enzyme to Treat Type 2 Diabetes Mellitus. *Trends in Endocrinology & Metabolism* **2016**, *27*, 24–34. doi:10.1016/j.tem.2015.11.003.
60. Sebokova, E.; Christ, A.; Boehringer, M.; Mizrahi, J. Dipeptidyl Peptidase IV Inhibitors: The Next Generation of New Promising Therapies for the Management of Type 2 Diabetes. *Current Topics in Medicinal Chemistry* **2007**, *7*, 547–555. doi:10.2174/156802607780091019.
61. Alafuzoff, I.; Aho, L.; Helisalmi, S.; Mannermaa, A.; Soininen, H. β-Amyloid deposition in brains of subjects with diabetes. *Neuropathology and Applied Neurobiology* **2009**, *35*, 60–68. doi:10.1111/j.1365-2990.2008.00948.x.
62. Zraika, S.; Hull, R.L.; Udayasankar, J.; Clark, A.; Utzschneider, K.M.; Tong, J.; Gerchman, F.; Kahn, S.E. Identification of the Amyloid-Degrading Enzyme Neprilysin in Mouse Islets and Potential Role in Islet Amyloidogenesis. *Diabetes* **2007**, *56*, 304–310. doi:10.2337/db06-0430.
63. Li, W. A Local Spherical Coordinate System Approach to Protein 3D Structure Description **2020**.
64. Li, W. Calcium Channel Trafficking Blocker Gabapentin Bound to the α-2-δ-1 Subunit of Voltage-Gated Calcium Channel: A Computational Structural Investigation **2020**.
65. Li, W.; Vottevor, G. Towards a Truly General Intermolecular Binding Affinity Calculator for Drug Discovery & Design **2023**. doi:10.20944/preprints202208.0213.v2.
66. Crunkhorn, S. Role of the Protein Data Bank. *Nature Reviews Drug Discovery* **2019**, *18*, 98–98. doi:10.1038/d41573-019-00010-1.
67. Westbrook, J.D.; Burley, S.K. How Structural Biologists and the Protein Data Bank Contributed to Recent FDA New Drug Approvals. *Structure* **2019**, *27*, 211–217. doi:10.1016/j.str.2018.11.007.
68. Li, W. Visualising the Experimentally Uncharted Territories of Membrane Protein Structures inside Protein Data Bank **2020**.
69. Wu, J.; Yan, Z.; Li, Z.; Qian, X.; Lu, S.; Dong, M.; Zhou, Q.; Yan, N. Structure of the voltage-gated calcium channel $Ca_V1.1$ at 3.6 Å resolution. *Nature* **2016**, *537*, 191–196.
70. Li, W.; Shi, G. How $Ca_V1.2$-bound verapamil blocks Ca^{2+} influx into cardiomyocyte: Atomic level views. *Pharmacological Research* **2019**, *139*, 153–157.